Adsorption (2013) 19:39–47
DOI 10.1007/s10450-012-9408-0

High-temperature hydrothermal synthesis of magnetically active, ordered mesoporous resin and carbon monoliths with reusable adsorption for organic dye

Fujian Liu · Hao Zhang · Longfeng Zhu · Yanmei Liao · Faisal Nawaz · Xiangju Meng · Feng-Shou Xiao

Received: 8 April 2011 / Accepted: 20 August 2012 / Published online: 6 September 2012

Abstract Magnetically active, thermally stable, and ordered mesoporous resin (MOMR-200) and carbon (MOMC-200) monoliths were prepared by one-pot hydrothermal synthesis from resol, copolymer surfactant, and iron cations at high-temperature (200 °C), followed by calcination at 360 °C and carbonization at 600 °C. X-ray diffraction results show that both MOMR-200 and MOMC-200 have ordered hexagonal mesoporous symmetry, and N_2 isotherms indicate that these samples have uniform mesopores (3.71, 3.45 nm), high surface area (328, 621 m^2/g) and large pore volume (0.31, 0.43 cm^3/g). Transmission electron microscopy shows that iron nanoparticles, which are superparamagnetic in nature, are dispersed in the network. More importantly, the high temperature (200 °C) products exhibit much better stability than the samples synthesized at low temperature (100 °C). Interestingly, MOMC-200 has higher adsorption capacity for organic dyes when compared with commercial adsorbents (activated carbon and macroporous resin: XAD-4). Combining the advantages such as magnetically active, thermally stable networks, ordered and open mesopores, high surface area, large pore volume, adsorption of pollutants in water and desorption in ethanol solvent, MOMC-200 is potentially important for water treatments.

Keywords High temperature synthesis · Ordered mesoporous carbon · Magnetically active · Adsorption · Stability

1 Introduction

Ordered mesoporous materials of silicas, metal oxides, carbon, and polymers have attracted much attention in the fields of catalysis, environmental technology, drug delivery, separation, and adsorption due to their advantages such as large surface area, tunable porosity, and uniform pore sizes (Kresge et al. 1992; Corma 1997; Wan and Zhao 2007; Yang et al. 1998; Liang et al. 2008). Mesoporous materials particularly silicas and carbon are effective adsorbents for the treatment of polluted water, but their relatively low hydrothermal stability and small particle sizes sometimes may prove problematic for industrial applications (Han et al. 2003; Li et al. 2004; Vinu et al. 2007). For example, relatively low hydrothermal stability of amorphous mesoporous silica walls is not favorable for retaining the mesostructure if treated with water; the small particle sizes result in the difficulty for separation of the mesoporous materials in liquid-solid phase processes (Lu et al. 2004a, 2004b; Teunissen et al. 2001).

It has been reported that ordered mesoporous materials of silicas, aluminosilicates, and polymers synthesized at high-temperatures could efficiently improve their stabilities (Xiao et al. 2009; Celer and Jaroniec 2006; Liu et al. 2009). For

Electronic supplementary material The online version of this article (doi:10.1007/s10450-012-9408-0) contains supplementary material, which is available to authorized users.

F. Liu
Institute of Applied Chemistry, Department of Chemistry, Shaoxing University, Huanchengxi Street 508, Shaoxing 312000, China

H. Zhang · L. Zhu · F. Nawaz
State Key Laboratory of Inorganic Synthesis and Preparative Chemistry and College of Chemistry, Jilin University, Qianjin Street 2699, Changchun 130012, P.R. China

Y. Liao · X. Meng · F.-S. Xiao (✉)
Key Lab of Applied Chemistry of Zhejiang Province, Department of Chemistry, Zhejiang University (XiXi Campus), Tianmushan Road 148, Hangzhou 310028, China
e-mail: fsxiao@mail.jlu.edu.cn

example, ordered mesoporous silica-based materials synthesized at the temperatures 180–230 °C have very high silica condensation, giving excellent hydrothermal and mechanical stabilities (Han et al. 2003; Wang et al. 2005; Celer and Jaroniec 2006); ordered mesoporous resins synthesized at 200–260 °C have superior cross-linking degree, exhibiting extraordinary thermal and mechanical stabilities (Liu et al. 2009). High-temperature route offers an opportunity to hydrothermally synthesize stable mesoporous materials.

Recently, a series of porous materials with good magnetic properties (such as magnetic mesoporous phenol-formaldehyde resin) have been successfully prepared (Sun et al. 2006; Zhai et al. 2009; Bourlinos et al. 2001; Gross et al. 2003; Lu et al. 2007; Wang and Dai 2009; Zhang et al. 2008), which opened a new door for magnetic separation by applying an appropriate magnetic field, however, the relative lower synthesized temperature (100 °C) will result in the lower cross-linking degree, further giving unstable networks of the samples (Liu et al. 2009); in the meanwhile, the low synthesized temperature can not make the iron species crystallization, only after carbonization at high temperature can make iron species crystallized into iron species, which may result in the aggregation of iron oxide nanoparticles. We demonstrate here a unique and controllable *one-pot* high temperature (200 °C) hydrothermal route for synthesizing magnetically active, highly thermally stable and ordered mesoporous phenol-formaldehyde resin (MOMR-x, where x stands for synthesis temperature) monoliths. These monoliths were synthesized at 200 °C in the presence of $FeCl_3$ and $FeSO_4$ using nonionic surfactant of P123 as a template, the high synthesized temperature can enhance the crystallization of iron species, resulting the better magnetic property of the as-synthesized samples. After carbonization at 600 °C, MOMR-x could be transformed into magnetically active and ordered mesoporous carbon (MOMC-x) monoliths.

2 Experimental procedures

2.1 Chemicals and synthesis of MOMR-x and MOMC-x

All reagents were analytical grade. Phenol, formaldehyde solution (38 wt.%), NaOH, ethanol, ferric chloride, ferrous sulfate, Rhodamine B (RhB), and activated carbon were obtained from Tianjin Guangfu Chemical Company. P123, XAD-4 were purchased from Sigma-Aldrich Company.

MOMR-x were prepared from hydrothermal synthesis under basic conditions. After carbonization, MOMR-x were transformed into MOMC-x. As a typical run, (1) 0.2 g of NaOH was dissolved in 10 mL of H_2O, followed by addition of 2.0 g phenol and 7 mL formaldehyde solution (38 wt.%). (2) After heating at 70–80 °C for 30–40 min, 20 mL of P123 (containing 1.5 g of P123) solution was added. (3) After heating at 80 °C for 2 h, the mixture was cooled down to room temperature. Then, the mixture was added dropwise into 20 mL of aqueous solution containing ferric chloride ($FeCl_3{\cdot}6H_2O$ 0.12 g, 0.44 mmol) and ferrous sulfate ($FeSO_4{\cdot}7H_2O$ 0.22 g, 0.88 mmol) under vigorous stirring. The molar ratio of $C_6H_5OH/CH_2O/Fe/NaOH/P123/H_2O$ in the mixture was 1/4.34/0.062/0.246/0.012/135.6. After further stirring for 30 min, the mixture was transferred to an autoclave. (4) When the autoclave was treated at 200 °C for 24 h, a black precipitate was observed at the bottom. (5) The solid MOMR-200 was obtained by washing with water and drying at 80 °C for 12 h. (6) After calcination at 360 °C under nitrogen for 5 h with a heating rate of 1 °C/min, P123 template in MOMR-200 could be removed. (7) Carbonization at 600 °C under N_2 condition for 2 h with a heating rate of 1 °C/min resulted in the formation of MOMC-200.

2.2 Characterization

Powder X-ray diffraction (XRD) patterns were recorded on Rigaku D/Max-2550 (wide-angle XRD) and Siemens D5005 diffractometer (small-angle XRD) using nickel-filtered Cu Kα radiation. N_2 isotherms were measured using a Micromeritics ASAP 2020M system at the liquid nitrogen temperature. The samples were outgassed for 10 h at 150 °C before the measurements. The pore-size distribution for mesopores was calculated using the Barrett-Joyner-Halenda (BJH) model. Thermogravimetric analysis (TG) was performed on a Perkin-Elmer TGA7 in flowing air, the heating rate was 20 °C/min. The magnetization curves were measured at 25 °C under a varying magnetic field with a Quantum Design MPMS-7 SQUID magnetometer. The UV-visible diffuse reflectance spectra were recorded on a Perkin-Elmer Lambda 20 UV/vis spectrometer, and the absorbance spectra were obtained from the reflectance spectra by means of Kubelka-Munk transformation. Transmission electron microscopy (TEM) experiments were performed on a JEM-3010 electron microscope (JEOL, Japan) with an acceleration voltage of 300 kV.

2.3 Adsorption of RhB

As typical run for measurement of adsorption capacity, 0.05 g of absorbent was added into 100 mL of RhB solution with the concentration of 40 ppm. After adsorption for 12 h under stirring at room temperature (22 °C), the absorbent was separated and the remaining solution was analyzed by UV spectroscopy at the wave length of 555 nm. The concentration of RhB in the solution was calculated from the reduction of the signal intensity (555 nm). During this process, the pH was kept neutral.

As typical run for detection of adsorptive kinetic curves, 0.1 g of absorbent was added into 25 mL of RhB solution

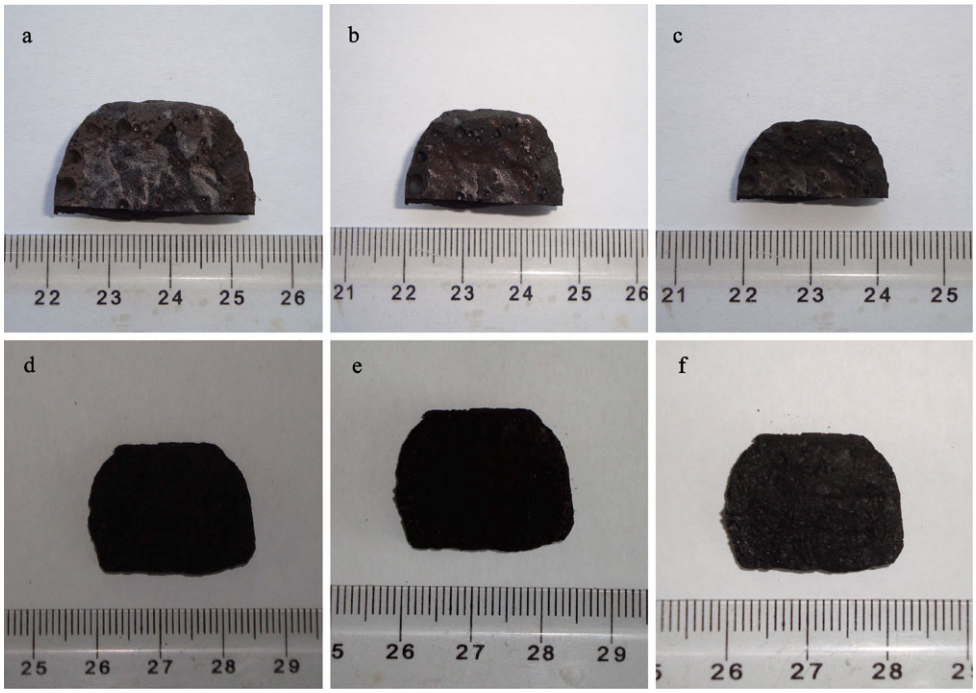

Fig. 1 Photographs of (**a**) as-synthesized MOMR-100, (**b**) MOMR-100 calcined at 360 °C in flowing N_2, (**c**) MOMC-100 carbonized at 600 °C in flowing N_2, (**d**) as-synthesized MOMR-200, (**e**) MOMR-200 calcined at 360 °C in flowing N_2, (**f**) MOMC-200 carbonized at 600 °C in flowing N_2

with the concentration of 40 ppm. After stirring at various times (10–480 min) at room temperature (22 °C), the solution was analyzed by UV spectroscopy at the wave length of 555 nm. The concentration of RhB in the solution was calculated from the reduction of the signal intensity. During this process, the pH was kept neutral.

3 Results and discussion

3.1 XRD

Figure 1 shows sample photographs of as-synthesized and calcined MOMR-x, and MOMC-x, giving monolith feature. Compared with as-synthesized samples, the volume of carbonized samples is significantly reduced, which is assigned to the shrinkage of polymer network in the samples by increasing temperature, and similar phenomenon is reported in literature (Zhang et al. 2005; Meng et al. 2005). For example, after calcination at 350 °C and carbonization at 600 °C, the length of MOMC-100 has been reduced for 31.8 %. In contrast, MOMC-200 has only 15.4 % contraction in the length by the same treatment. These results are reasonably attributed to that MOMR-200 has much better cross-linking degree than MOMR-100 (Liu et al. 2009).

Figure 2A shows small-angle XRD patterns of MOMR-x and MOMC-x. As-synthesized MOMR-x samples only show one peak. MOMR-100 and MOMR-200 give the peak at 0.846° and 0.740°, respectively. Compared with as-synthesized samples, calcined MOMR-x samples exhibit strong peak intensity and mesostructure ordering, giving two peaks indexed as (100) and (110) reflections associated with 2-D hexagonal symmetry (Zhao et al. 1998a, 1998b). After calcination at 360 °C for 5 h, MOMR-100 and MOMR-200 give the peak for (100) direction at 0.896 and 0.760°, respectively. After carbonization of MOMR-x, MOMC-x clearly show peak shifts associated with ordered hexagonal mesoporous arrays. The peak for (100) direction for MOMC-100 and MOMC-200 is at 1.01 and 0.91°, respectively.

It is worth noting that both MOMR-200 and MOMC-200 have larger d values than MOMR-100 and MOMC-100. For example, MOMR-100 and MOMC-100 show d (100) value at 9.96 and 8.74 nm, while MOMR-200 and MOMC-200 exhibit the value at 11.6 and 9.70 nm, respectively. This phenomenon is possibly attributed to the difference in self-assembly of P123 with resol at distinguishable temperatures.

Figure 2B shows wide-angle XRD patterns of MOMR-x and MOMC-x. Notably, there is no peak for as-synthesized MOMR-100, indicating no crystalline iron oxides. However, as-synthesized MOMR-200 shows obvious peaks associated with crystalline γ-Fe_2O_3 (Sun et al. 2006; Yi et al. 2006). Calcination at 360 °C results in the appearance of peaks associated with γ-Fe_2O_3. Compared with MOMR-x, MOMC-x samples exhibit weak peak intensity associated with γ-Fe_2O_3 and new peaks related to α-Fe (Sun et al. 2006; Yi et al. 2006), suggesting the reduction of γ-Fe_2O_3 crystal size and appearance of new phase of α-Fe by the interaction between γ-Fe_2O_3 with carbon species. The existence of α-Fe in the samples is very helpful for magnetically active property (Sun et al. 2006; Yi et al. 2006).

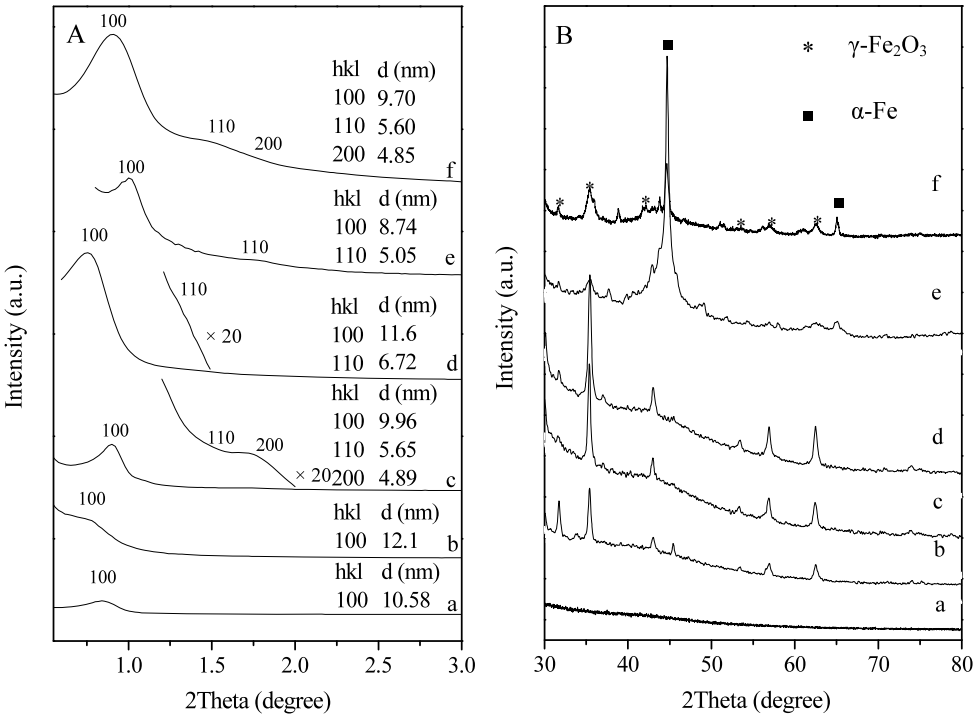

Fig. 2 (**A**) Small angle and (**B**) wide angle XRD patterns of as-synthesized (*a*) MOMR-100 and (*b*) MOMR-200, (*c*) MOMR-100 and (*d*) MOMR-200 calcined at 360 °C for 5 h in flowing N_2, (*e*) MOMR-100 and (*f*) MOMR-200 carbonized at 600 °C for 2 h in flowing N_2

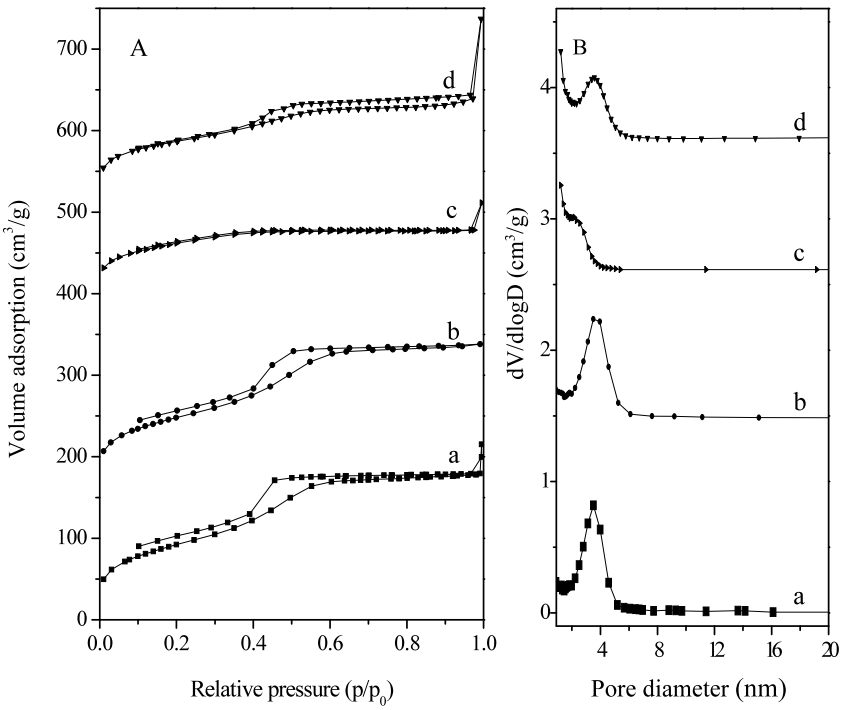

Fig. 3 (**A**) N_2 adsorption/desorption isotherms and (**B**) the corresponding pore size distribution of (*a*) MOMR-100 and (*b*) MOMR-200 calcined at 360 °C for 5 h in flowing N_2, (*c*) MOMC-100 and (*d*) MOMC-200 carbonized at 600 °C for 2 h in flowing N_2. The isotherms for (*b–d*) are offset by 150, 300 and 400 cm^3/g along the *vertical axis* for clarity; The pore size curves for (*b–d*) are also offset by 0.5, 1.5 and 2 cm^3/g along the *vertical axis* for clarity, respectively

Figure S1 (see electronic supplementary material) shows small-angle and wide-angle XRD patterns of MOMR-100 and MOMC-100 with increasing iron loading. The results exhibit that these samples still have good mesostructured ordering.

3.2 N_2 isotherms

Figure 3 shows N_2 isotherms and BJH pore size distribution of various samples. Calcined MOMR-100 and MOMR-200 (Fig. 3A) exhibit similar isotherms, giving

Table 1 Textural properties of calcined MOMRs, MOMCs, activated carbon, and XAD-4

Samples	$D_{(100)}$ (nm)	S_{BET}[a] (m^2/g)	V_p[a] (cm^3/g)	D_p[b] (nm)	Wall thickness (nm)
MOMR-100	10.0	335	0.34	3.50	6.5
MOMR-200	11.6	328	0.31	3.71	7.9
MOMC-100	8.7	556	0.23	2.30	6.4
MOMC-200	9.7	621	0.43	3.45	6.3
Activated carbon	–	722	0.38	<1	–
XAD-4	–	790	0.81	2–100	–

[a]BET surface areas and pore volumes determined from N_2 adsorption isotherms at −196 °C

[b]Pore size distribution estimated from BJH model

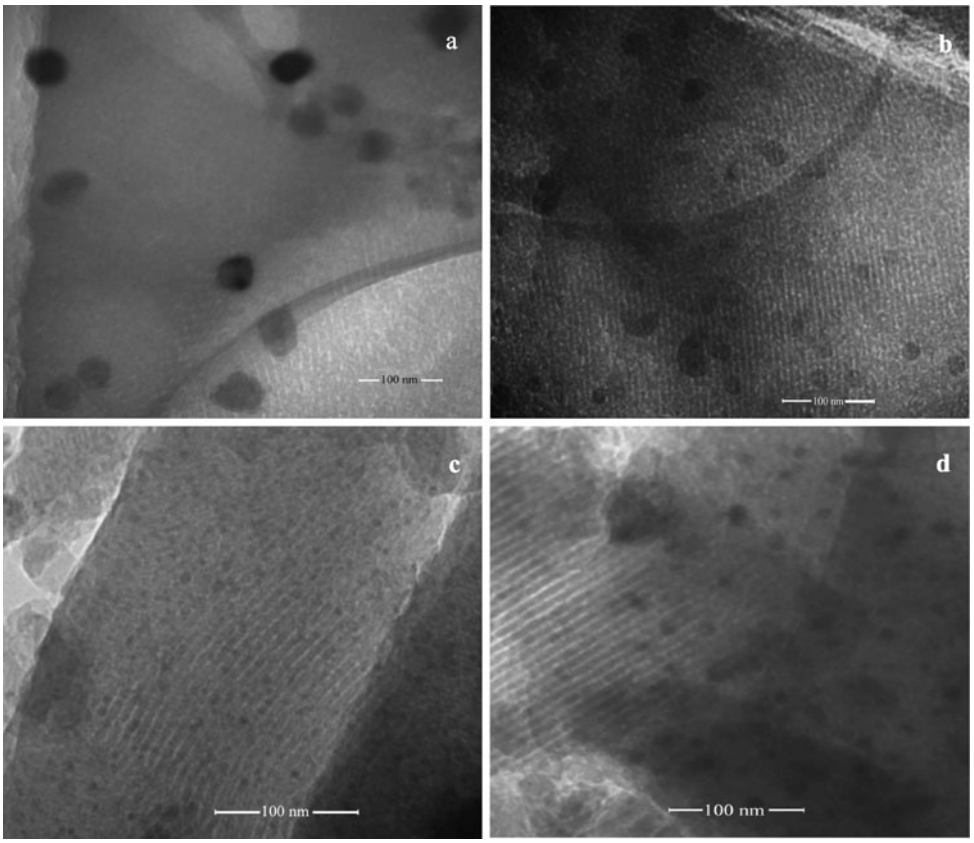

Fig. 4 TEM images of (**a**) MOMR-100 and (**b**) MOMR-200 calcined at 360 °C for 5 h in flowing N_2, (**c**) MOMC-100 and (**d**) MOMC-200 carbonized at 600 °C for 2 h in flowing N_2

a sharp capillary condensation step at $P/P_0 = 0.4$–0.6, which is due to the presence of mesopores (Zhao et al. 1998a, 1998b). Correspondingly, the pore sizes are ranged at 3.5–3.7 nm. However, after carbonization of MOMR-x, MOMC-100 and MOMC-200 have different isotherms, showing the pore size distribution at 2.2 and 3.45 nm, respectively. Clearly, the pore size distribution of MOMC-100 is much smaller than that of MOMR-100, which is related to the relatively easy contraction of flexible polymer network in MOMR-100 with low cross-linking degree [24]. On the contrary, MOMC-200 and MOMR-200 have almost the same pore size distribution, which is assigned to the rigid polymer network in MOMR-200 with high cross-linking degree (Liu et al. 2009). These results suggest that high-temperature synthesis of MOMC-200 is very favorable for retaining the mesostructure during carbonization of MOMR-200.

We also observe the changes in pore volume and surface area of the samples synthesized at different temperatures. MOMR-100 and MOMR-200 have similar pore volume (0.34 and 0.31 cm^3/g) and Brunauer-Emmett-Teller (BET) surface area (335 and 328 m^2/g). However, after the same carbonization, the pore volume (0.43 cm^3/g) and BET surface area (621 m^2/g) of MOMC-200 are absolutely higher than those (0.25 cm^3/g and 556 m^2/g) of MOMC-100. Apparently, high-temperature synthesis of MOMR-x is very helpful for preparation of MOMC-x with high BET surface area and large pore volume.

Table 1 briefly presents the sample parameters. Notably, MOMR-100 and MOMC-100 have d value at 9.96 and

8.74 nm and pore size distribution at 3.50 and 2.30 nm, giving the pore thickness at 6.46 and 6.44 nm, respectively. These results suggest that the shift of *d* values by carbonization of the samples is mainly resulted from the change in the mesopores. In contrast, MOMR-200 and MOMC-200 have *d* value at 11.60 and 9.7 nm and pore size distribution at 3.71 and 3.45 nm, giving the pore wall thickness at 7.89 and 6.25 nm, respectively. These results suggest that the shift of *d* values by carbonization of the samples is mainly related to the contraction of polymer walls.

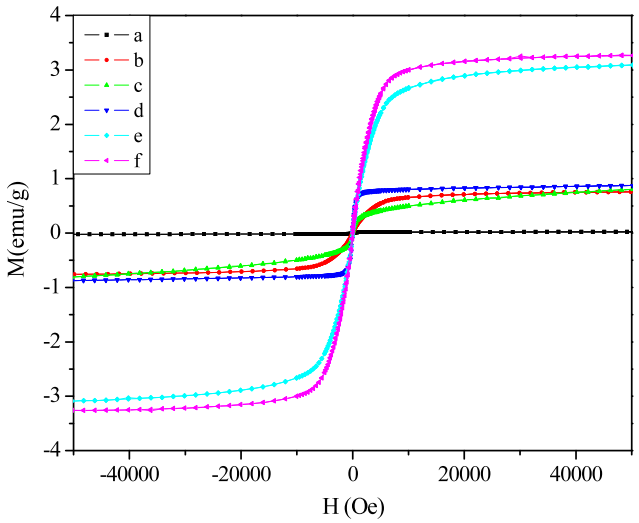

Fig. 5 Magnetization curves of as-synthesized (*a*) MOMR-100 and (*b*) MOMR-200, (*c*) MOMR-100 and (*d*) MOMR-200 calcined at 360 °C for 5 h in flowing N_2, (*e*) MOMC-100 and (*f*) MOMC-200 carbonized at 600 °C for 2 h in flowing N_2

Figure S2 shows N_2 isotherms of MOMR-100 and MOMC-100 with increasing iron loading. These samples still exhibit type-IV adsorption associated with mesostructure, but their BET surface areas (152 and 454 m^2/g) and pore volumes (0.14 and 0.20 cm^3/g) are reduced significantly due to the increase of iron loading.

3.3 TEM

Figure 4 shows TEM images of calcined MOMR-*x* and carbonized MOMC-*x* viewed from (110) direction. These images exhibits good ordering, in agreement with XRD results (Fig. 2). Interestingly, the uniform nanoparticles of Fe_2O_3 or α-Fe are highly dispersed in the network of polymer or carbon. Fe_2O_3 particle sizes in MOMR-*x* are mainly ranged at 20–50 nm. After carbonization, MOMC-*x* samples have nanoparticles of Fe_2O_3 or α-Fe mainly distributed at 3–6 nm. Compared with those in MOMR-*x*, the particle sizes of iron species in MOMC-*x* reduce significantly, which is well consistent with wide-angle XRD results (Fig. 2B).

It is considered that iron source is introduced into the samples due to the strong coordination between iron cations with phenols [41]. After calcination at 360 °C or carbonization at 600 °C, iron cations in the samples are aggregated with each other, forming nanoparticles of Fe_2O_3 or α-Fe.

3.4 Magnetic property

Figure 5 shows room-temperature magnetization curves of calcined MOMR-*x* and carbonized MOMC-*x*. As-synthesized MOMR-100 has no magnetic property, which is due

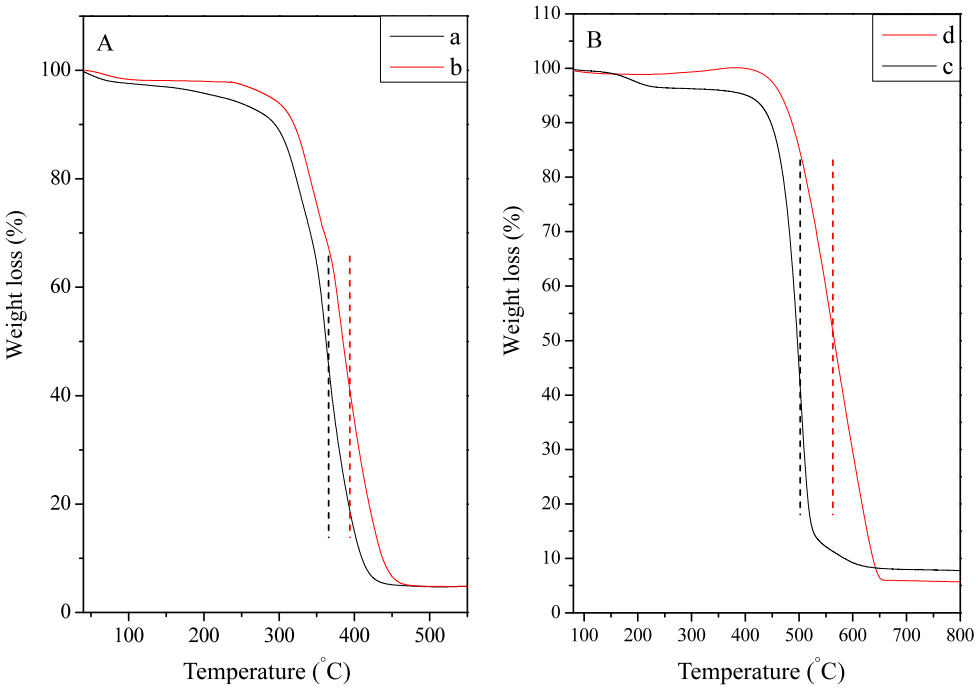

Fig. 6 TG curves of (**A**) as-synthesized (*a*) MOMR-100 and (*b*) MOMR-200 and (**B**) carbonized (*c*) MOMC-100, (*d*) MOMC-200

to the absence of crystalline iron species. As-synthesized MOMR-200 shows weak magnetization, giving the saturation value at 0.78 emu/g due to the presence of γ-Fe_2O_3. After calcination at 360 °C, both MOMR-100 and MOMR-200 still show weak magnetization (0.8 and 0.89 emu/g). Compared with calcined samples, MOMC-x show relatively strong saturation magnetization (3.1 and 3.3 emu/g), which are reasonably related to the formation of α-Fe during carbonization of MOMR-x. Notably, these samples have not hysteresis loop, suggesting their superparamagnetic property (Zhao et al. 2005).

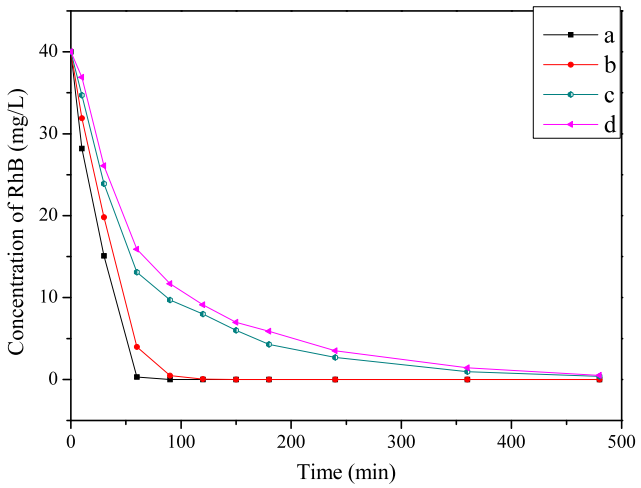

Fig. 7 Dynamic adsorption of RhB in water over (*a*) MOMC-200, (*b*) Activated carbon, (*c*) MOMR-200, and (*d*) XAD-4

3.5 Thermal stabilities of the samples

Figure 6A shows TG curves of as-synthesized MOMR-100 and MOMR-200. Both samples exhibit the weight loss at 50–280, 295–355, and 355–450 °C, which are attributed to the desorption of air and water, decomposition of the copolymer template P123 and destruction of the polymer network, respectively [11, 24]. Interestingly, the decomposition of MOMR-200 (center at 390 °C) is higher than that of MOMR-100 (center at 365 °C), which is due to the higher cross-linking degree obtained as a results of synthesis at high temperature (Liu et al. 2009).

Figure 6B shows TG curves of MOMC-100 and MOMC-200, giving the weight loss mainly distributed at 430–620 °C, which are attributed to the combustion of the carbon in the air (Su et al. 2005; Fröba et al. 1999). Notably, MOMC-200 has much higher combustion temperature (center at 560 °C) than MOMC-100 (center at 500 °C), demonstrating that MOMC-200 has much better thermal stability than MOMC-100.

3.6 Adsorption of organic dye

As a model pollutant, RhB is chosen as an adsorbate for the adsorption and desorption experiments. Figure 7 shows dynamic adsorption of RhB in water over various samples. By comparing the textural parameters (Table 1), XAD-4 consisted of polystyrene and polydivinylbenzene is a commercial polymer adsorbent (BET surface area of 790 m^2/g, pore sizes of 2–100 nm, pore volume of 0.81 cm^3/g), and it takes

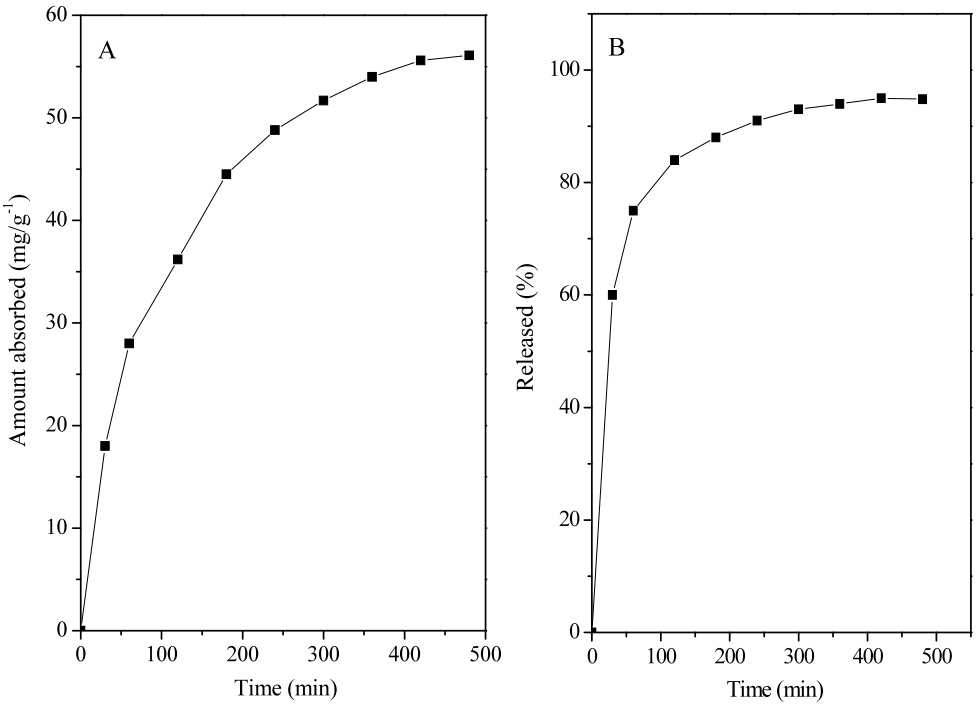

Fig. 8 Dynamic adsorption and desorption of RhB in (**A**) water and (**B**) ethanol over MOMC-200

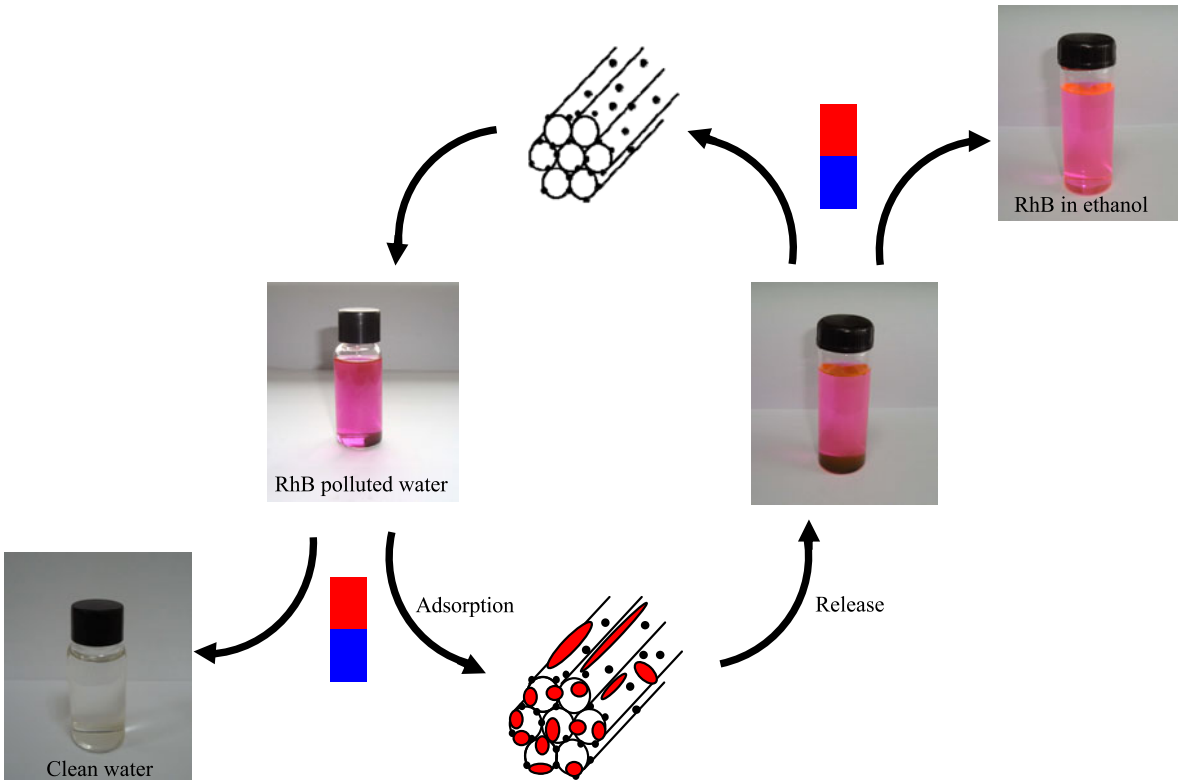

Fig. 9 Proposed scheme for removal of organic dyes in water by magnetically active and ordered mesoporous MOMC-200

for over 480 min for complete adsorption of RhB in water. In contrast, calcined MOMR-200 has a higher adsorption rate than XAD-4. Interestingly, MOMC-200 has the highest adsorption rate. When the adsorption time is about 90 min, whole amount of RhB in water was fully adsorbed, its adsorption rate is faster than that of a commercial activated carbon, although its BET surface area (621 m^2/g) and pore volume (0.43 cm^3/g) are less than those (722 m^2/g and 0.38 cm^3/g) of the activated carbon. By comparing the textural parameters of activated carbon and MOMC-200, it is suggested that relatively large, open, and ordered mesopores are important for adsorption of RhB dye on the adsorbents.

Furthermore, we measured the adsorption capacity of RhB on MOMC-200 (56.4 mg/g, Fig. 8A), which is obviously higher than a commercial activated carbon (44.1 mg/g). More importantly, the adsorbed RhB is almost released in ethanol solvent. After desorption for 6 h, nearly 95 % adsorbed RhB was released into the ethanol (Fig. 8B). This feature is potentially helpful for adsorption-desorption recycles of RhB by magnetic activity process (Fig. 9), and the steps are in the following: (1) fresh MOMC-200 is added into the polluted water to adsorb organic dye; (2) adsorbed MOMC-200 is separated by the magnetic field, producing a clear water; (3) after desorption of adsorbed dye, regenerated MOMC-200 is separated again; (4) the regenerated MOMC-200 could be used to adsorb the pollutants in the next recycle. After five recycles, MOMC-200 still shows almost the same adsorption amount for RhB.

4 Conclusions

Thermally stable MOMR-*x* monoliths have been successfully synthesized from high-temperature (200 °C) assembly of resol with P123 in the presence of iron cations. After removal of the surfactant by calcination at 360 °C, the magnetic resin with open mesopores is obtained. After carbonization at 600 °C in flowing nitrogen, thermally stable MOMC-*x* monoliths are formed. Interestingly, both the MOMR-*x* and MOMC-*x* exhibit good adsorption capacity for organic dye. Particularly, MOMC-200 even shows much better adsorption capacity than a commercial activated carbon. These efficient materials potentially offer an alternative approach for cleaning polluted water.

Acknowledgements This work is supported by the State Basic Research Project of China (2009CB623507) and National Natural Science Foundation of China (20973079).

References

Bourlinos, A.B., Simopoulos, A., Boukos, N., Petridis, D.: Magnetic modification of the external surfaces in the MCM-41 porous sil-

ica: synthesis, characterization, and functionalization. J. Phys. Chem. B **105**, 7432–7437 (2001)
Celer, E.B., Jaroniec, M.: Temperature-programmed microwave-assisted synthesis of SBA-15 ordered mesoporous silica. J. Am. Chem. Soc. **128**, 14408–14414 (2006)
Corma, A.: From microporous to mesoporous molecular sieve materials and their use in catalysis. Chem. Rev. **97**, 2373–2419 (1997)
Fröba, M., Köhn, R., Bouffaud, G.: Fe_2O_3 nanoparticles within mesoporous MCM-48 silica: in situ formation and characterization. Chem. Mater. **11**, 2858–2865 (1999)
Gross, A.F., Diehl, M.R., Beverly, K.C., Richman, E.K., Tolbert, S.H.: Controlling magnetic coupling between cobalt nanoparticles through nanoscale confinement in hexagonal mesoporous silica. J. Phys. Chem. B **107**, 5475–5482 (2003)
Han, Y., Li, D.F., Zhao, L., Song, J.W., Yang, X.Y., Li, N., Di, Y., Li, C.J., Wu, S., Xu, X.Z., Meng, X.J., Lin, K.F., Xiao, F.S.: High-temperature generalized synthesis of stable ordered mesoporous silica-based materials by using fluorocarbon-hydrocarbon surfactant mixtures. Angew. Chem. Int. Ed. **42**, 3633–3637 (2003)
Kresge, C.T., Leonowicz, M.E., Roth, W.J., Vartuli, J.C., Beck, J.S.: Ordered mesoporous molecular sieves synthesized by a liquid-template mechanism. Nature **359**, 710–712 (1992)
Li, D., Han, Y., Song, J.W., Zhao, L., Xu, X.Z., Di, Y., Xiao, F.S.: High-temperature synthesis of stable ordered mesoporous silica materials by using fluorocarbon–hydrocarbon surfactant mixtures. Chem. Eur. J. **10**, 5911–5922 (2004)
Liang, C.D., Li, Z.J., Dai, S.: Mesoporous carbon materials synthesis and modification. Angew. Chem. Int. Ed. **47**, 3696–3717 (2008)
Liu, F.J., Li, C.J., Ren, L.M., Meng, X.J., Zhang, H., Xiao, F.-S.: High-temperature synthesis of stable and ordered mesoporous polymer monoliths with low dielectric constants. J. Mater. Chem. **19**, 7921–7928 (2009)
Lu, A.H., Schmidt, W., Matoussevitch, N., Bŏnnemann, H., Spliethoff, B., Tesche, B., Bill, E., Kiefer, W., Schüth, F.: Nanoengineering of a magnetically separable hydrogenation catalyst. Angew. Chem. Int. Ed. **43**, 4303–4306 (2004a)
Lu, A.H., Li, W.C., Kiefer, A., Schmidt, W., Bill, E., Fink, G., Schüth, F.: Fabrication of magnetically separable mesostructured silica with an open pore system. J. Am. Chem. Soc. **126**, 8616–8617 (2004b)
Lu, A.H., Salabas, E.L., Schüth, F.: Magnetic nanoparticles: synthesis, protection, functionalization, and application. Angew. Chem. Int. Ed. **46**, 1222–1224 (2007)
Meng, Y., Gu, D., Zhang, F.Q., Shi, Y.F., Yang, H.F., Li, Z., Yu, C.Z., Tu, B., Zhao, D.Y.: Ordered mesoporous polymers and homologous carbon frameworks amphiphilic surfactant templating and direct transformation. Angew. Chem. Int. Ed. **44**, 7053–7059 (2005)
Su, F.B., Zeng, J.H., Bao, X.Y., Yu, Y.S., Lee, J.Y., Zhao, X.S.: Preparation and characterization of highly ordered graphitic mesoporous carbon as a Pt catalyst support for direct methanol fuel cells. Chem. Mater. **17**, 3960–3967 (2005)
Sun, Z.H., Wang, L.F., Liu, P.P., Wang, S.C., Sun, B., Jiang, D.Z., Xiao, F.-S.: Magnetically motive porous sphere composite and its excellent properties for the removal of pollutants in water by adsorption and desorption cycles. Adv. Mater. **18**, 1968–1971 (2006)
Teunissen, W., Grootde, F.M.F., Geus, J., Stephan, O., Tence, M., Colliex, C.: The structure of carbon encapsulated NiFe nanoparticles. J. Catal. **204**, 169–174 (2001)
Vinu, A., Srinivasu, P., Takahashi, M., Mori, T., Balasubramanian, V.V.: Controlling the textural parameters of mesoporous carbon materials. Ariga K. Microporous Mesoporous Mater. **100**, 20–26 (2007)
Wan, Y., Zhao, D.Y.: On the controllable soft-templating approach to mesoporous silicates. Chem. Rev. **107**, 2821–2860 (2007)
Wang, X.Q., Dai, S.: A simple method to ordered mesoporous carbons containing nickel nanoparticles. Adsorption **15**, 138–144 (2009)
Wang, L.F., Lin, K.F., Di, Y., Zhang, D.L., Li, C.J., Yang, Q., Yin, C.Y., Sun, Z.H., Jiang, D.Z., Xiao, F.-S.: High-temperature synthesis of stable ordered mesoporous silica materials using mesoporous carbon as a hard template. Microporous Mesoporous Mater. **86**, 81 (2005)
Xiao, N., Wang, L., Zou, Y.C., Wang, C.Y., Ji, Y.Y., Song, J.W., Li, F., Meng, X.J., Xiao, F.S.: High-temperature synthesis of ordered mesoporous silicas from solo hydrocarbon surfactants and understanding of their synthetic mechanisms. J. Mater. Chem. **19**, 661–665 (2009)
Yang, P.D., Zhao, D.Y., Margolese, D.I., Chmelka, B.F., Stucky, G.D.: Generalized syntheses of large-pore mesoporous metal oxides with semicrystalline frameworks. Nature **396**, 152–155 (1998)
Yi, D.K., Lee, S.S., Papaefthymiou, G.C., Ying, J.Y.: Nanoparticle architectures templated by SiO_2/Fe_2O_3 nanocomposites. Chem. Mater. **18**, 614–619 (2006)
Zhai, Y.P., Dou, Y.Q., Liu, X.X., Tu, B., Zhao, D.Y.: One-pot synthesis of magnetically separable ordered mesoporous carbon. J. Mater. Chem. **19**, 3292–3300 (2009)
Zhang, F.Q., Meng, Y., Gu, D., Yan, Y., Yu, C.Z., Tu, B., Zhao, D.Y.: A facile aqueous route to synthesize highly ordered mesoporous polymers and carbon frameworks with iad bicontinuous cubic structure. J. Am. Chem. Soc. **127**, 13508–13509 (2005)
Zhang, L., Qiao, S.Z., Jin, Y.G., Chen, Z.G., Gu, H.C., Lu, G.Q.: Magnetic hollow spheres of periodic mesoporous organosilica and Fe_3O_4 nanocrystals: fabrication and structure control. Adv. Mater. **20**, 805–809 (2008)
Zhao, D.Y., Feng, J.L., Huo, Q.S., Melosh, N., Fredrickson, G.H., Chmelka, B.F., Stucky, G.D.: Triblock copolymer syntheses of mesoporous silica with periodic 50 to 300 angstrom pores. Science **279**, 548–552 (1998a)
Zhao, D.Y., Huo, Q.S., Feng, J.L., Chmelka, B.F., Stucky, G.D.: Nonionic triblock and star diblock copolymer and oligomeric surfactant syntheses of highly ordered, hydrothermally stable, mesoporous silica structures. J. Am. Chem. Soc. **120**, 6024–6036 (1998b)
Zhao, W., Gu, J., Zhang, L., Chen, H., Shi, J.: Fabrication of uniform magnetic nanocomposite spheres with a magnetic core/mesoporous silica shell structure. J. Am. Chem. Soc. **127**, 8916–8917 (2005)